



**Formation of coordination polymer glass by mechanical milling: dependence on metal ions and molecular doping for H<sup>+</sup> conductivity**

Journal:	<i>ChemComm</i>
Manuscript ID	CC-COM-03-2018-002399.R1
Article Type:	Communication

SCHOLARONE™  
Manuscripts

## Formation of coordination polymer glass by mechanical milling: dependence on metal ions and molecular doping for H<sup>+</sup> conductivity

Received 00th January 20xx,  
Accepted 00th January 20xx

DOI: 10.1039/x0xx00000x

www.rsc.org/

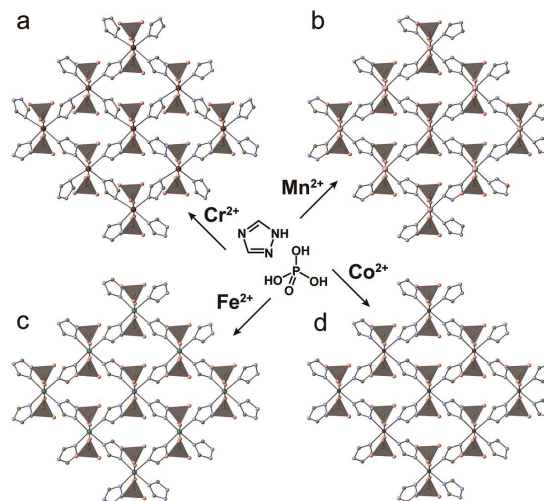
Yuki Ohara,<sup>a</sup> Akira Hinokimoto,<sup>a</sup> Wenqian Chen,<sup>a</sup> Takashi Kitao,<sup>a</sup> Yusuke Nishiyama,<sup>b,c</sup> You-lee Hong,<sup>c</sup> Susumu Kitagawa,<sup>d</sup> and Satoshi Horike\*<sup>a,d,e</sup>

**Four isostructural coordination polymer crystals having different metal ions were synthesized and studied for ball milling-induced glass formation. Distinct glass formation was discussed from crystal structures. Doping of molecules for CP glass during the milling was demonstrated, and it resulted tunable glass properties ( $T_g$  and  $T_c$ ) and enhancement of anhydrous H<sup>+</sup> conductivity.**

Glass shows distinct character from crystal, and there are many advantages of glass as a functional material. Tunability of composition, structural isotropy, mechanical flexibility, and optical transparency are the examples.<sup>1</sup> Exploring the new types of glass is of significant challenge for both fundamental science and industrial application. Coordination polymer (CP) crystals are constructed from metal ions and bridging ligands to form extended structure.<sup>2</sup> Usually they are crystalline state, and show attractive functions including gas storage, catalysis, sensor, and conductivity. On the other hand, the glass science of CP is rarely studied despite their potential, and more works on synthesizing new CP glasses or elucidation of glass formation mechanism are demanded.<sup>3</sup> To prepare the glassy state of CP, melt-quenching or mechanical milling are attempted.<sup>4, 5</sup> Former approach is common for other solid materials but this is yet limited for most of CP crystals, because of the difficulty to show stable liquid state. Latter approach is the direct preparation of glassy state from crystal, and it could be applicable for wider range of CP crystals. Meanwhile, only one report exists about the vitrification by mechanical milling.<sup>4</sup> Understanding which CP crystals could be glassy state by

mechanical milling, and how can we modulate the property of glassy state, is the important discussion for exploring the CP glasses. In this study, we synthesized four isostructural two-dimensional (2D) CP crystals each of them has different metal ions, and studied the behaviour of vitrification by ball milling. We also demonstrated chemical modification of CP glass by doping organic molecule during the mechanical vitrification, and it resulted improvement of anhydrous proton (H<sup>+</sup>) conductivity.

2D CPs, [M<sup>2+</sup>(1,2,4-triazole)<sub>2</sub>(H<sub>2</sub>PO<sub>4</sub>)<sub>2</sub>] (named as MTz, M = Cr, Mn, Fe, Co) were synthesized by mechanochemical or solvothermal reactions. All the crystal structures were determined by single crystal X-ray diffraction (Figure 1). CrTz is monoclinic and MnTz, FeTz, CoTz are orthorhombic. Each metal ion is coordinated to four N atoms of 1,2,4-triazole in equatorial position and two O atoms of H<sub>2</sub>PO<sub>4</sub><sup>-</sup> in the axial position to form octahedral coordination geometry and resultant layers are stacked along the *c* axis with hydrogen bonds. We previously reported [M<sup>2+</sup>(1,2,4-triazole)<sub>2</sub>(H<sub>2</sub>PO<sub>4</sub>)<sub>2</sub>] (M = Zn or Cd), and CdTz transforms to glassy state by ball milling, whereas ZnTz does not.<sup>4, 6</sup>



<sup>a</sup> Department of Synthetic Chemistry and Biological Chemistry, Graduate School of Engineering, Kyoto University, Katsura, Nishikyō-ku, Kyoto 615-8510, Japan

<sup>b</sup> RIKEN CLST-JEOL Collaboration Center, Tsurumi, Yokohama, Kanagawa 230-0045, Japan

<sup>c</sup> JEOL RESONANCE Inc., 3-1-2 Musashino, Akishima, Tokyo 196-8558, Japan

<sup>d</sup> Institute for Integrated Cell-Material Sciences (WPI-icEMS), Institute for Advanced Study, Kyoto University, Yoshida-Honmachi, Sakyo-ku, Kyoto 606-8501, Japan

<sup>e</sup> AIST-Kyoto University Chemical Energy Materials Open Innovation Laboratory (ChEM-OIL), Yoshida-Honmachi, Sakyo-ku, Kyoto 606-8501, Japan

† Footnotes relating to the title and/or authors should appear here.

Electronic Supplementary Information (ESI) available: [Experimental detail, crystallographic data, PXRD, SSNMR, TGA, TGA-MS, IR, sample photo]. See DOI: 10.1039/x0xx00000x

Figure 1. Single crystal structures of (a) CrTz (b) MnTz (c) FeTz (d) CoTz. C and N are grey and sky blue.  $\text{H}_2\text{PO}_4^-$  are shown as tetrahedral.

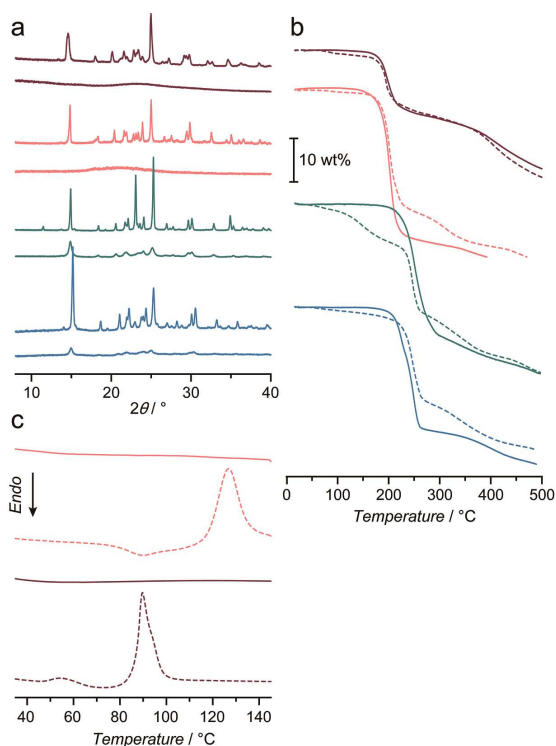


Figure 2. (a) PXRD of (upper) before and (below) after ball milling (b) TGA profiles before (solid line) and after (dot line) ball milling. CrTz (dark red), MnTz (pink), FeTz (green), CoTz (blue). (c) DSC profiles before (solid line) and after (dot line) ball milling for CrTz (dark red), MnTz (pink). Heating rates are  $10 \text{ K min}^{-1}$ .

We confirmed good match of the experimental powder X-ray diffraction patterns (PXRD) and simulated patterns from crystal structures for CrTz, MnTz, FeTz, CoTz (Figure S1). To study the mechanical vitrification, we applied solvent-free ball milling for the four crystalline samples under Ar atmosphere. We applied 120 minutes for CrTz, and 240 minutes for MnTz, FeTz, CoTz for milling, and denote the ball milled samples as MTz' (M = Cr, Mn, Fe, Co). To check the feature of glassy state, PXRD and thermogravimetric analysis (TGA) were measured for the four MTz'. As shown in Figure 2a, FeTz' and CoTz' retain the peaks in PXRD, even though their intensity are smaller than those of FeTz and CoTz. TGA profiles of FeTz' and CoTz' show gradual weight loss start at  $70^\circ\text{C}$  and their thermal stabilities become lower than FeTz and CoTz (Figure 2b). Increase the milling time did not improve the amorphization. From the results, FeTz and CoTz do not form glassy state under the investigated condition. On the other hand, PXRD of CrTz' and MnTz' are typical amorphous which do not have any Bragg diffraction. TGA suggests CrTz' and MnTz' show similar temperatures to start weight loss with their crystalline states. DSC for CrTz' (milled for 120 minutes) and MnTz' (milled for 240 minutes) are shown in Figure 2c. As we observed in CdTz previously,<sup>4</sup> both CrTz' and MnTz' show glass transition ( $T_g$ ) and crystallization ( $T_c$ ).  $T_g$  and  $T_c$  for CrTz' and MnTz' are  $62, 90, 81, 128^\circ\text{C}$ , respectively. As a result, we elucidate CrTz and MnTz form

glassy state, whereas FeTz and CoTz do not under the investigated ball milling condition. The distinct behaviour of glass formation and dependence on metal ion in MTz would be discussed from the crystal structures. As shown in Table S1, Metal-N (from 1,2,4-triazole) bond lengths for CrTz ( $2.138\text{--}2.343 \text{ \AA}$ ) and MnTz ( $2.224\text{--}2.283 \text{ \AA}$ ) are larger than those of FeTz ( $2.181\text{--}2.190 \text{ \AA}$ ) and CoTz ( $2.129\text{--}2.167 \text{ \AA}$ ). ZnTz which does not form glassy state by ball milling also has short bond length ( $2.134\text{--}2.182 \text{ \AA}$ ).<sup>6</sup> This is explained from ionic radius of each metal ion. We assume that the glass forming CrTz and MnTz prefer to show plastic deformation by ball milling because of lower energy of coordination bonds. Higher bonding energies for FeTz, CoTz, and ZnTz lead the materials to be brittle, and it does not allow the vitrification.

We studied the structure of MnTz' by Mn K-edge X-ray adsorption and pair distribution function (PDF) from PXRD collected at Synchrotron (Figure 3a–3c). XANES spectra of MnTz and MnTz' are identical suggesting the valence state and coordination geometry of Mn in MnTz' is unchanged by the vitrification. Radial distribution function from EXAFS spectrum suggests that the first nearest neighbouring atoms of  $\text{Mn}^{2+}$  in MnTz' is same as MnTz (below  $2.4 \text{ \AA}$ ), but the second or higher neighbouring atoms are disordered in MnTz' because of low intensity of the corresponding peaks. Simulation of RDF from single crystal structure has not been successful because of the overlap of peak assignments.

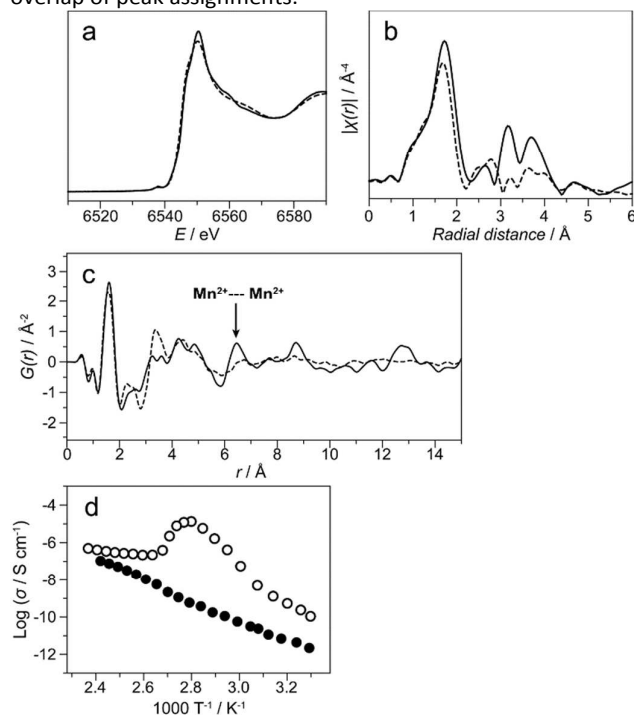


Figure 3. (a) XANES spectra (b) Fourier transform of the EXAFS spectra (c) PDF spectra of MnTz (solid line) and MnTz' (dot line). (d) Temperature dependent  $\text{H}^+$  conductivity under anhydrous condition for MnTz (solid circle) and MnTz' (open circle).

PDF of MnTz and MnTz' suggests the consistent conclusion with XAS. We found correlated peaks for MnTz' at  $r < 5.0 \text{ \AA}$ , and the peak of Mn-Mn at  $6.45 \text{ \AA}$  in MnTz' significantly diminishes. IR spectra of MnTz and MnTz' are identical (Figure

S2), though the peaks of MnTz' are broad because of the structural disorder, and the results suggest local coordination bonds of  $Mn^{2+}$  to  $H_2PO_4^-$  or 1,2,4-triazole in MnTz' are preserved to form octahedral geometry, but the ligand orientations are distorted. The distorted network of MnTz' leads our interest for  $H^+$  conductivity because of the dynamics of protonic species ( $H_2PO_4^-$  or 1,2,4-triazole) in the glassy state. CP or metal organic framework (MOF) are expected for new class of  $H^+$  conductors, and design of anhydrous  $H^+$  conductivity is one of big challenge for fuel cell technology.<sup>7</sup> Figure 3d shows temperature-dependent  $H^+$  conductivity plots of MnTz and MnTz' by AC impedance spectroscopy under an anhydrous condition. In contrast to the negligible conductivity of MnTz, MnTz' shows about two order higher conductivity than MnTz at 25 °C, and the conductivity reaches  $1.3 \times 10^{-5} \text{ S cm}^{-1}$  at 86 °C which is four order higher than that of MnTz. MnTz' starts recrystallization above  $T_c$  and it turns to the same crystal structure of MnTz checked by PXRD (Figure S3).<sup>8</sup> We denote the recrystallized state from glassy state as MnTz'' (and MTz'' for others). Because of the re-ordering of structure as crystallization,  $H^+$  conductivity decreases but it does not back to the same conductivity as heating. This is presumably because MnTz'' contains amorphous region or defects in the structure which facilitates the  $H^+$  migration.<sup>9</sup>

Another interest is how to control the property of CP glass by chemical modification. To investigate the possibility of chemical doping for CP glass, we employed CdTz which is known to transform glassy state by ball milling as same as CrTz and MnTz.<sup>4</sup> We conducted ball milling-induced vitrification of CdTz for 240 minutes under the co-presence of diazabicyclo[2,2,2]octane (dabco) with the molar ratios of 0.05 and 0.10 per  $Cd^{2+}$  in CdTz (Figure 4a). Dabco is selected as a dopant because of its sublimation property, high Lewis basicity, and small size. After the ball milling for 240 minutes under Ar atmosphere, both samples (we denote CdTz'-0.05dabco and CdTz'-0.10dabco, respectively) showed complete amorphous patterns in PXRD (Figure 4b). No peak attributed by dabco crystal is observed. TGA and DSC profiles for CdTz, CdTz' which was prepared by the ball milling for 240 minutes, CdTz'-0.05dabco, CdTz'-0.10dabco are shown in Figure S4 and Figure 4c. All four samples show comparable thermal stability by TGA. Note dabco itself shows quick drop from 25 °C because of sublimation.  $T_g$  and  $T_c$  by DSC vary as increase the doping amount of dabco compared with CdTz'.  $T_g$  for CdTz', CdTz'-0.05dabco, CdTz'-0.10dabco are 87, 92, 96 °C and  $T_c$  for these are 123, 132, 135 °C, respectively. The trend of  $T_g$  is observed in the other glass materials such as metals and molecular alloys.<sup>10</sup>

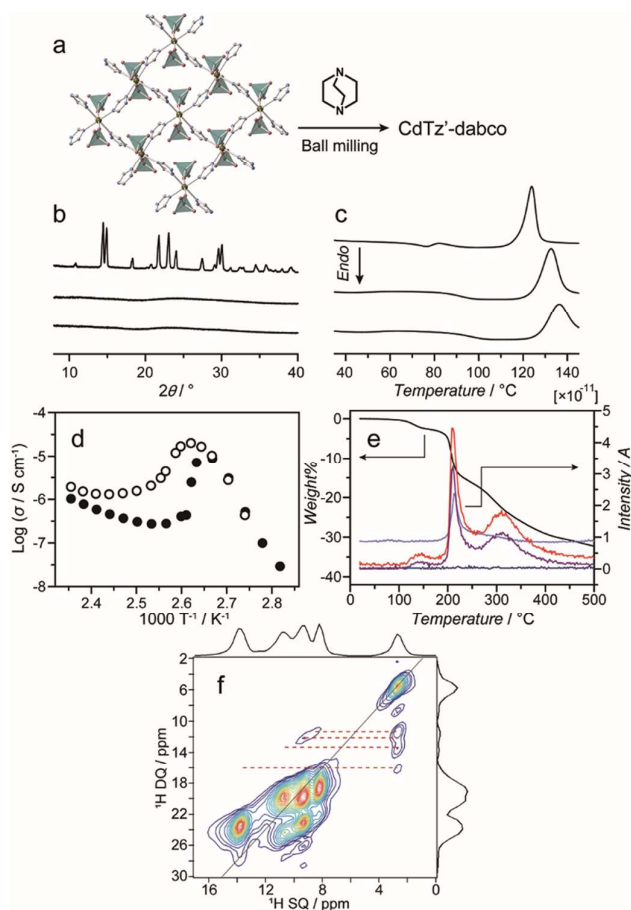


Figure 4. (a) Scheme of preparation of CdTz'-xdabco ( $x = 0.05, 0.10$ ). (b) PXRD of CdTz (upper), CdTz'-0.05dabco (middle), CdTz'-0.10dabco (bottom). (c) DSC of CdTz' (upper), CdTz'-0.05dabco (middle), CdTz'-0.10dabco (bottom). (d) Temperature dependent  $H^+$  conductivity under an anhydrous condition for CdTz' (solid circle) and CdTz'-0.10dabco (open circle). (e) TGA-MS profiles of CdTz'-0.10dabco. Weight change (black), peaks of  $m/z = 18$  (pale purple), 42 (red), 55 (dark blue), 69 (purple). (f) 2D  $^1H$  DQ/ $^1H$  SQ solid state NMR spectrum of CdTz'-0.10dabco.

Observation of single  $T_g$  and  $T_c$  for CdTz'-0.05dabco and CdTz'-0.10dabco represents that dabco are uniformly distributed in CdTz'-0.05dabco or CdTz'-0.10dabco, and the doping influences the glass transition and crystallization behaviours. Because CdTz'-0.05dabco and CdTz'-0.10dabco have sufficient thermal stability and distinct features of  $T_g$  and  $T_c$  with CrTz',  $H^+$  conductivity were measured (Figure 4d). Observed conductivities of CdTz' and CdTz'-0.10dabco are similar from 25 to 100 °C and these are much higher than those of CdTz. Thanks to the dabco doping, the temperature for the maximum conductivity for CdTz'-0.10dabco is larger than that of CdTz' because of higher  $T_g$ , and resulting maximum conductivity at 108 °C is  $2.0 \times 10^{-5} \text{ S cm}^{-1}$  which is two times higher than the maximum conductivity of CdTz' at 103 °C. CdTz'-0.10dabco shows crystallization above  $T_c$  to return to the original 2D structure as we confirmed by PXRD (Figure S5). Conductivity of CdTz''-0.10dabco which is crystallized above  $T_c$  decreases because of the recovery of structural order, but the values are retained to be high compared with the case of CdTz' above  $T_c$ . CdTz''-0.10dabco shows over one order higher

conductivity than CdTz'' at 115 °C, even though both show same PXRD patterns. The improved H<sup>+</sup> conductivity for CdTz''-0.10dabco than CdTz'' is because of the doping effect of dabco. To study the chemical environment of dabco in CdTz''-0.10dabco, we measured solid state NMR (Figure 4f and S5). <sup>1</sup>H, <sup>13</sup>C, <sup>15</sup>N, <sup>31</sup>P and <sup>113</sup>Cd resonances (Figure S6) of the backbone structure of CdTz''-0.10dabco in one (1D) and two (2D) dimensional NMR spectra appear at the same position as those of CdTz, suggesting that the recrystallization does not influence the backbone structure. Additional correlation related to dabco appears in those spectra of CdTz''-0.10dabco. <sup>1</sup>H double quantum (DQ)/single quantum (SQ) spectra (Figure 4f) indicates the proton proximity, giving the correlation peaks between the protons of dabco (2.7 ppm) and the protons of 1,2,4-triazole (8.2, 9.3 and 13.8 ppm) as well as of OH group of H<sub>2</sub>PO<sub>4</sub><sup>-</sup> (10.7 ppm). In addition, the weak but definite correlation of dabco/<sup>113</sup>Cd and dabco/<sup>31</sup>P is also observed in 2D <sup>1</sup>H-<sup>113</sup>Cd and <sup>1</sup>H-<sup>31</sup>P heteronuclear correlation (HETCOR) spectrum. The results indicate the doped dabco locate near 1,2,4-triazole in the 2D network approximately within 4 Å, but keep away from Cd and P atoms. Note the CdTz does not have guest-accessible channels from the crystal structure, but the treatment of ball milling-induced vitrification with dopant, and crystallization by heating is able to provide homogeneously doped crystal.

As solid-state NMR suggests the mutual interaction of dabco and 2D network in CrTz''-0.10dabco, we measured TGA-MS for CdTz'-0.10dabco and CdTz to estimate the thermal stability of trapped dabco (Figure 4e). As a reference we also measured 1,2,4-triazole and dabco and each shows *mz* = 42/69, and *mz* = 42/55, respectively (Figure S7). CdTz shows clear two-step weight loss at 190 and 300 °C, and MS suggests they are 1,2,4-triazole. CdTz'-0.10dabco transforms to CdTz''-0.10dabco above *T<sub>c</sub>* and the crystallized state shows small MS peaks at 150 °C which is attributed by 1,2,4-triazole, and subsequently larger peak of 1,2,4-triazole at 200 °C accompanied with the peak of H<sub>2</sub>O (*mz* = 18). The water is probably because of the sample's hydrophilicity and the handling under the air. Interestingly, CdTz''-0.10dabco does not show any release of dabco to 500 °C, as we do not observe corresponding peak (*mz* = 55). This suggests the doped dabco are strongly bound in CdTz'-0.10dabco which is the crystallized form. Please note that the result of elemental analysis for CdTz'-0.10dabco well matches with the theoretical values (CNH), and the glass sample contains stoichiometric amount of dabco. Solid-state NMR and TGA-MS also support the sub-nano scale dispersion of dabco in CdTz''-0.10dabco and the homogeneously doped structure is feasible by mechanical vitrification and accompanying crystallization.

## Conclusions

We synthesized four isostructural 2D CP crystals having different transition metal ions (Cr<sup>2+</sup>, Mn<sup>2+</sup>, Fe<sup>2+</sup>, Co<sup>2+</sup>), and demonstrated the ball milling-induced glass formation. Cr<sup>2+</sup> and Mn<sup>2+</sup> crystals transformed to stable glassy states and the distinguishable glass formation behaviour was discussed from the original crystal structures. We also studied the chemical

doping during the mechanical vitrification by ball mill, and observed tunable properties of glass transition temperature (*T<sub>g</sub>*) and crystallization temperature (*T<sub>c</sub>*). Distribution of the doped molecules is studied by solid-state NMR and TGA-MS. They are strongly trapped in the framework to change the property of CP glass. As a result, significant enhancement of anhydrous H<sup>+</sup> conductivity was observed. The results showed the wide applicability of ball milling to create CP glass, and further modification of the property of CP glass by chemical doping.

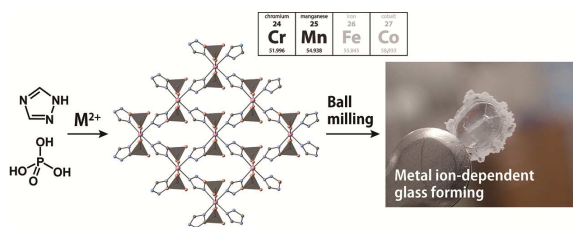
## Conflicts of interest

There are no conflicts to declare.

## Notes and references

‡ This work was supported by "Molecular Technology" of Strategic International Collaborative Research Program (SICORP) from the Japan Science and Technology Agency (JST). WPI-iCeMS is supported by World Premier International Research Initiative (WPI), MEXT, Japan. We thank Ms. Nanae Shimanaka for X-ray diffraction analysis, and Synchrotron facilities in Japan (SPring-8, BL02B2 beamline for PXRD and Aichi Synchrotron BL551 beamline for XAS).

1. P. Boolchand and W. J. Bresser. *Nature*, 2001, **410**, 1070; Q. H. Shi, J. F. Wang, J. P. Zhang, J. Fan and G. D. Stucky. *Adv. Mater.*, 2006, **18**, 1038; J. Haines, C. Levelut, A. Isambert, P. Hebert, S. Kohara, D. A. Keen, T. Hammouda and D. Andrault. *J. Am. Chem. Soc.*, 2009, **131**, 12333; D. C. Hofmann. *Science*, 2010, **329**, 1294.
2. H. Furukawa, K. E. Cordova, M. O'Keeffe and O. M. Yaghi. *Science*, 2013, **341**, 1230444; H. C. Zhou and S. Kitagawa. *Chem. Soc. Rev.*, 2014, **43**, 5415; A. J. Howarth, Y. Liu, P. Li, Z. Li, T. C. Wang, J. T. Hupp and O. K. Farha. *Nat. Rev. Mater.*, 2016, **1**, 15018.
3. D. Umeyama, S. Horike, M. Inukai, T. Itakura and S. Kitagawa. *J. Am. Chem. Soc.*, 2015, **137**, 864; Y. Zhao, S. Y. Lee, N. Becknell, O. M. Yaghi and C. A. Angell. *J. Am. Chem. Soc.*, 2016, **138**, 10818; H. Z. Tao, T. D. Bennett and Y. Z. Yue. *Adv. Mater.*, 2017, **29**.
4. W. Chen, S. Horike, D. Umeyama, N. Ogiwara, T. Itakura, C. Tassel, Y. Goto, H. Kageyama and S. Kitagawa. *Angew. Chem. Int. Ed.*, 2016, **55**, 5195.
5. T. D. Bennett, Y. Yue, P. Li, A. Qiao, H. Tao, N. G. Greaves, T. Richards, G. I. Lampronti, S. A. Redfern, F. Blanc, O. K. Farha, J. T. Hupp, A. K. Cheetham and D. A. Keen. *J. Am. Chem. Soc.*, 2016, **138**, 3484.
6. D. Umeyama, S. Horike, M. Inukai, T. Itakura and S. Kitagawa. *J. Am. Chem. Soc.*, 2012, **134**, 12780.
7. J. M. Taylor, T. Komatsu, S. Dekura, K. Otsubo, M. Takata and H. Kitagawa. *J. Am. Chem. Soc.*, 2015, **137**, 11498; S. Kim, B. Joarder, J. A. Hurd, J. Zhang, K. W. Dawson, B. S. Gelfand, N. E. Wong and G. K. H. Shimizu. *J. Am. Chem. Soc.*, 2018.
8. Note the values of *T<sub>g</sub>* are different from that determined by DSC and PXRD, because of different heating rates of the measurements.
9. T. Panda, S. Horike, K. Hagi, N. Ogiwara, K. Kadota, T. Itakura, M. Tsujimoto and S. Kitagawa. *Angew. Chem. Int. Ed.*, 2017, **56**, 2413.
10. L. Schultz. *Mater. Sci. Eng.*, 1988, **97**, 15; M. Nagahama, H. Suga and O. Andersson. *Thermochim. Acta*, 2000, **363**, 165.



Metal ion-dependent glass formation of coordination polymer crystals and direct molecular doping for the glass are studied with  $H^+$  conductivity.